



1       **Simulation of ozone-vegetation coupling and feedback in**  
2                   **China using multiple ozone damage schemes**

3  
4  
5  
6

Jiachen Cao<sup>1</sup>, Xu Yue<sup>1\*</sup>, Mingrui Ma<sup>2</sup>

- 7    1. Jiangsu Key Laboratory of Atmospheric Environment Monitoring and Pollution  
8    Control, Collaborative Innovation Center of Atmospheric Environment and  
9    Equipment Technology, School of Environmental Science and Engineering, Nanjing  
10   University of Information Science & Technology (NUIST), Nanjing, 210044, China  
11   2. State Key Laboratory of Pollution Control and Resource Reuse, School of the  
12   Environment, Nanjing University, Nanjing, 210044, China

13  
14  
15

16   \*Corresponding author: Xu Yue

17   email: [yuxu@nuist.edu.cn](mailto:yuxu@nuist.edu.cn)

18  
19  
20  
21  
22  
23  
24



25

### Abstract

26 As a phytotoxic pollutant, surface ozone ( $O_3$ ) not only affects plant physiology but  
27 also influences meteorological fields and air quality by altering leaf stomatal  
28 functions. Previous studies revealed strong feedbacks of  $O_3$ -vegetation coupling in  
29 China but with large uncertainties due to the applications of varied  $O_3$  damage  
30 schemes and chemistry-vegetation models. In this study, we quantify the  $O_3$   
31 vegetation damage and the consequent feedbacks to surface meteorology and air  
32 quality in China by coupling two  $O_3$  damage schemes (S2007 vs. L2013) into a fully  
33 coupled regional meteorology-chemistry model. With different schemes and  
34 damaging sensitivities, surface  $O_3$  is predicted to decrease summertime gross primary  
35 productivity by 5.5%-21.4% and transpiration by 5.4%-23.2% in China, in which the  
36 L2013 scheme yields 2.5-4 times of losses relative to the S2007 scheme. The damages  
37 to photosynthesis of sunlit leaves are ~2.6 times that of shaded leaves in the S2007  
38 scheme but show limited differences in the L2013 scheme. Though with large  
39 discrepancies in offline responses, the two schemes yield similar magnitude of  
40 feedback to surface meteorology and  $O_3$  air quality. The  $O_3$ -induced damage to  
41 transpiration increases national sensible heat by 3.2-6.0  $W m^{-2}$  (8.9% to 16.2%) while  
42 reduces latent heat by 3.3-6.4  $W m^{-2}$  (-5.6% to -17.4%), leading to a 0.2-0.51  $^{\circ}C$   
43 increase in surface air temperature and a 2.2-3.9% reduction in relative humidity.  
44 Meanwhile, surface  $O_3$  concentrations on average increase by 1.3-3.3  $\mu g m^{-3}$  due to  
45 the inhibitions of stomatal uptake and the anomalous enhancement in isoprene  
46 emissions, the latter of which is attributed to the surface warming by  $O_3$ -vegetation  
47 coupling. Our results highlight the importance of  $O_3$  control in China due to its  
48 adverse effects on ecosystem functions, deterioration of global warming, and  
49 exacerbation of  $O_3$  pollution through the  $O_3$ -vegetation coupling.

50

51 **Keywords:** Ozone, vegetation, feedback, meteorology, air quality, regional model

52



## 53 **1 Introduction**

54 Surface ozone ( $O_3$ ) is one of the most enduring air pollutants affecting air quality  
55 in China, with detrimental effects on human health and ecosystem functions (Monk et  
56 al., 2015). Long-term observations and numerical simulations have shown that  $O_3$   
57 affects stomatal conductance (Li et al., 2017), accelerates vegetation aging (Feng et al.,  
58 2015), and reduces photosynthesis (Wittig et al., 2007). These negative effects altered  
59 carbon allocation (Yue and Unger, 2014; Lombardozzi et al., 2015) and inhibited plant  
60 growth (Li et al., 2016), leading to a decreased strength of ecosystem carbon uptake  
61 (Ainsworth, 2012). Moreover, these effects have profound implications for  
62 global/regional climate and atmospheric environment. Given the significant  
63 ecological impacts, a systematic quantification of the  $O_3$  vegetation damage effect in  
64 China is of great importance for the better understanding of the side effects of  $O_3$   
65 pollution on both regional carbon uptake and climate change.

66 At present, field experiments on  $O_3$ -induced vegetation damage have been  
67 conducted in China but were mostly confined to individual monitoring sites. For  
68 instance, Su et al. (2017) conducted experiments on grassland in Inner Mongolia and  
69 found that elevated  $O_3$  concentrations resulted in a decrease of approximately 20% in  
70 the photosynthetic rate of herbaceous plants. Meta-analysis of tropical, subtropical,  
71 and temperate tree species in China found that increased  $O_3$  concentrations reduced  
72 net photosynthesis and total biomass of Chinese woody plants by 28% and 14%,  
73 respectively (Li et al., 2017). However, most of these experiments were conducted  
74 using open-top chambers with artificially controlled  $O_3$  concentrations, rather than  
75 actual surface  $O_3$  concentrations, making it difficult to quantitatively estimate the  
76 impact of ambient  $O_3$  on vegetation productivity. Furthermore, the spatial coverage of  
77 field experiments is limited, which hinders the direct use of observational data for  
78 assessing  $O_3$  vegetation damage in different regions of China.

79 Alternatively, numerical models provide a more feasible approach to quantify the  
80  $O_3$ -induced vegetation damage from the regional to global scales. Currently, there are  
81 three main parameterizations for the calculation of ozone vegetation damage. Felzer et



82 al. (2004) established an empirical scheme based on the Accumulated Ozone exposure  
83 over a Threshold of 40 ppb (AOT40) within the framework of a terrestrial ecosystem  
84 model. They further estimated that O<sub>3</sub> pollution in the United States led to a decrease  
85 in net primary productivity (NPP) by 2.6% to 6.8% during the period of 1980-1990.  
86 However, the AOT40 is related to O<sub>3</sub> concentrations alone and ignores the biological  
87 regulations on the O<sub>3</sub> stomatal uptake, leading to inconsistent tendencies between O<sub>3</sub>  
88 pollution level and plant damage at the drought conditions (Gong et al., 2021). In  
89 acknowledge of such deficit, Sitch et al. (2007) proposed a semi-mechanistic scheme  
90 calculating O<sub>3</sub> vegetation damage based on the stomatal uptake of O<sub>3</sub> fluxes and the  
91 coupling between stomatal conductance and leaf photosynthesis. Yue and Unger  
92 (2014) implemented this scheme into the Yale Interactive terrestrial Biosphere (YIBs)  
93 model. Taking into account varied O<sub>3</sub> sensitivities of different vegetation types, they  
94 estimated that surface O<sub>3</sub> led to reductions of 2-5% in the summer gross primary  
95 productivity (GPP) in eastern U.S. from 1998 to 2007. Later, Lombardozzi et al.  
96 (2013) conducted a meta-analysis using published chamber data and found different  
97 levels of responses to O<sub>3</sub> exposure between stomatal conductance and photosynthesis.  
98 They further implemented the independent response relationships into the Community  
99 Land Model (CLM) and estimated that current ozone levels led to a reduction in  
100 global GPP by 8%-12% (Lombardozzi et al., 2015).

101 The O<sub>3</sub> stress on vegetation physiology can feed back to affect regional climate.  
102 Lombardozzi et al. (2015) employed the CLM model and found that current O<sub>3</sub>  
103 exposure reduced transpiration by 2%-2.4% globally and up to 15% regionally over  
104 eastern U.S., Europe, and Southeast Asia, leading to further perturbations in surface  
105 energy and runoff. In U.S., Li et al. (2016) found that the O<sub>3</sub> vegetation damage  
106 reduced latent heat (LH) flux, precipitation, and runoff by 10-27 W m<sup>-2</sup>, 0.9-1.4 mm  
107 d<sup>-1</sup>, and 0.1-0.17 mm d<sup>-1</sup>, respectively, but increased surface air temperature by  
108 0.6-2.0 °C during the summer of 2007-2012. In China, Zhu et al. (2022) performed  
109 simulations and found that the inclusion of O<sub>3</sub>-vegetation interaction caused a 5-30 W  
110 m<sup>-2</sup> decrease in LH, 0.2-0.8 °C increase in surface air temperature, and 3% reduction



111 in relative humidity during summers of 2014-2017. Recently, Jin et al. (2023) applied  
112 a different regional model and estimated that O<sub>3</sub> exposure weakened plant  
113 transpiration and altered surface heat flux in China, resulting in significant increase of  
114 up to 0.16 °C in maximum daytime temperature and decrease of -0.74% in relative  
115 humidity. However, all these previous estimates of O<sub>3</sub>-induced feedback to climate  
116 were derived using the empirical O<sub>3</sub> damage scheme proposed by Lombardozzi et al.  
117 (2013), which assumed fixed damage ratios independent of O<sub>3</sub> dose for some  
118 vegetation species and as a result may have biases in the further estimated feedback to  
119 climate.

120 The O<sub>3</sub>-vegetation coupling also has intricate implications for air quality. On one  
121 hand, O<sub>3</sub>-vegetation coupling can influence meteorological conditions that affect O<sub>3</sub>  
122 generation, ultimately influencing the O<sub>3</sub> level (Sadiq et al., 2017). On the other hand,  
123 it can also influence biogenic emissions and dry deposition, thereby affecting O<sub>3</sub>  
124 concentrations (Gong et al., 2020). Sadiq et al. (2017) implemented O<sub>3</sub>-vegetation  
125 coupling in the Community Earth System Model (CESM) and estimated that surface  
126 O<sub>3</sub> concentrations increased 4-6 ppb in Europe, North America, and China due to  
127 O<sub>3</sub>-vegetation coupling. By using the CLM model with the empirical scheme of  
128 Lombardozzi et al. (2013), Zhou et al. (2018) found that O<sub>3</sub>-induced damage on leaf  
129 area index (LAI) could lead to changes in global O<sub>3</sub> concentrations by -1.8 to +3 ppb  
130 in boreal summer. Gong et al., (2020) used the O<sub>3</sub> damage scheme from Sitch et al.  
131 (2007) embedded in a global climate-chemistry-carbon coupled model and estimated  
132 that O<sub>3</sub>-induced stomatal inhibition led to an average surface O<sub>3</sub> increase of 1.2-2.1  
133 ppb in eastern China and 1.0-1.3 ppb in western Europe. Different from the above  
134 global simulations with coarse resolutions, regional modeling with fine resolution can  
135 reveal more details about O<sub>3</sub>-vegetation coupling and feedback to surface O<sub>3</sub>  
136 concentrations in China (Zhu et al., 2022; Jin et al., 2023). However, all these regional  
137 simulations were carried out using O<sub>3</sub> damage scheme of Lombardozzi et al. (2013),  
138 limiting the exploration of model uncertainties due to varied O<sub>3</sub> vegetation damage  
139 schemes.



140 In this study, we implemented O<sub>3</sub> vegetation damage schemes from both Sitch et  
141 al. (2007) and Lombardozzi et al. (2013) into the widely-used regional  
142 meteorology-chemistry model WRF-Chem. We validated the simulated meteorology  
143 and O<sub>3</sub> concentrations, and performed sensitivity experiments to explore the O<sub>3</sub>  
144 damage to GPP and consequent feedbacks to regional climate and air quality in China.  
145 Within the same framework, we compared the differences of O<sub>3</sub>-vegetation coupling  
146 from two schemes and explored the causes for the discrepancies. We aimed to  
147 quantify the modeling uncertainties in the up-to-date estimates of O<sub>3</sub> impact on  
148 regional carbon fluxes and its feedback to regional climate and air quality in China.

149

## 150 **2 Method**

### 151 **2.1 WRF-Chem model**

152 We used WRF-Chem model version 3.9.1 to simulate meteorological fields and  
153 O<sub>3</sub> concentration in China. The model includes atmospheric physics and dynamical  
154 processes, atmospheric chemistry, and biophysical and biochemical processes (Grell  
155 et al., 2005, Skamarock et al., 2008). The model domain is configured with 196×160  
156 grid cells at 27 km horizontal resolution on the Lambert conformal projection, and  
157 covers the entire mainland China. In the vertical direction, 28 layers are set extending  
158 from surface to 50 hPa. The meteorological initial and boundary conditions were  
159 adopted from ERA5 reanalysis produced by the European Centre for Medium-Range  
160 Weather Forecasts (ECMWF) at a horizontal resolution of 0.25°×0.25° (Hersbach et al.,  
161 2020). The chemical initial and boundary conditions were generated from the Model  
162 for Ozone and Related Chemical Tracer version 4 (MOZART-4), which is available at  
163 a horizontal resolution of 1.9°×2.5° with 56 vertical layers (Emmons et al., 2010).

164 Anthropogenic emissions are adopted from the 0.25° Multi-resolution Emission  
165 Inventory for China (MEIC) and MIX Asian emission inventory for the other regions  
166 (available at <http://meicmodel.org>). Biogenic emissions are calculated online using  
167 the Model of Emissions of Gases and Aerosols from Nature (Guenther et al., 2006),  
168 which considers the impacts of plant types, weather conditions, and leaf area on



169 vegetation emissions. Atmospheric chemistry is simulated using the Carbon Bond  
170 Mechanism version Z (CBMZ) (Zaveri and Peters, 1999) gas-phase chemistry module  
171 coupled with a four-bin sectional Model for Simulating Aerosol Interactions and  
172 Chemistry (MOSAIC) (Zaveri et al., 2008). The photolysis scheme is based on the  
173 Madronich Fast-TUV photolysis module (Tie et al., 2003). The physical  
174 configurations include the Morrison double-moment microphysics scheme (Morrison  
175 et al., 2009), the Grell-3 cumulus scheme (Grell et al., 2002), the Rapid Radiative  
176 Transfer Model longwave radiation scheme (Mlawer et al., 1997), the Goddard  
177 short-wave radiation scheme (Chou and Suarez, 1994), the Yonsei University  
178 planetary boundary layer scheme (Hong et al., 2006), and the revised MM5 (Fifth  
179 generation Mesoscale Model) Monin–Obukhov surface layer scheme.

180

## 181 **2.2 Noah-MP model**

182 Noah-MP is a land surface model coupled to WRF-Chem with multiple options  
183 for key land-atmosphere interaction processes (Niu et al., 2011). Noah-MP considers  
184 canopy structure with canopy height and crown radius, and depicts leaves with  
185 prescribed dimensions, orientation, density, and radiometric properties. The model  
186 employs a two-stream radiative transfer approach for surface energy and water  
187 transfer processes (Dickinson, 1983). Noah-MP is capable of distinguishing  
188 photosynthesis pathways between C<sub>3</sub> and C<sub>4</sub> plants, and defines vegetation-specific  
189 parameters for leaf photosynthesis and respiration.

190 Noah-MP considers prognostic vegetation growth through the coupling between  
191 photosynthesis and stomatal conductance (Farquhar et al., 1980; Ball et al., 1987).  
192 The photosynthesis rate,  $A$  ( $\mu\text{molCO}_2 \text{ m}^{-2} \text{ s}^{-1}$ ), is calculated as one of three limiting  
193 factors as follows:

$$194 \quad A_{tot} = \min(W_c, W_j, W_e) I_{gs}$$

195 (1)

196 where  $W_c$  is the RuBisco-limited photosynthesis rate,  $W_j$  is the light-limited  
197 photosynthesis rate, and  $W_e$  is the export-limited photosynthesis rate.  $I_{gs}$  is the



198 growing season index with values ranging from 0 to 1. Stomatal conductance ( $g_s$ ) is  
199 computed based on photosynthetic rate as follows:

$$200 \quad g_s = \frac{1}{r_s} = m \frac{A_{net}}{C_s} RH + b \quad (2)$$

201 where  $b$  is the minimum stomatal conductance;  $m$  is the Ball-Berry slope of the  
202 conductance-photosynthesis relationship;  $A_{net}$  is the net photosynthesis by subtracting  
203 dark respiration from  $A_{tot}$ ;  $C_s$  is the ambient CO<sub>2</sub> concentration at the leaf surface.  
204 The assimilated carbon is allocated to various parts of vegetation (leaf, stem, wood,  
205 and root) and soil carbon pools (fast and slow), which determines the variations of  
206 LAI and canopy height. Plant transpiration rate is then estimated using the dynamic  
207 LAI and stomatal conductance. Noah-MP also distinguishes the photosynthesis of  
208 sunlit and shaded leaves. Sunlit leaves are more limited by CO<sub>2</sub> concentration while  
209 shaded leaves are more constrained by insolation, leading to varied responses to O<sub>3</sub>  
210 damage.

211

### 212 **2.3 Scheme for ozone damage on vegetation**

213 We implemented the O<sub>3</sub> vegetation damage schemes proposed by Sitch et al.  
214 (2007) (thereafter S2007) and Lombardozzi et al. (2013) (thereafter L2013) into the  
215 Noah-MP. In S2007 scheme, the undamaged fraction  $F$  for net photosynthesis is  
216 dependent on the sensitivity parameter  $a_{PFT}$  and excessive area-based stomatal O<sub>3</sub> flux,  
217 which is calculated as the difference between  $f_{O_3}$  and threshold  $y_{PFT}$ :

$$218 \quad F = 1 - a_{PFT} \times \max\{f_{O_3} - y_{PFT}, 0\} \quad (3)$$

219 where  $a_{PFT}$  and  $y_{PFT}$  are specifically determined for individual plant functional types  
220 (PFTs) based on measurements (Table 1). The stomatal O<sub>3</sub> flux  $f_{O_3}$  is calculated as

$$221 \quad f_{O_3} = \frac{[O_3]}{r_a + k_{O_3} \cdot r_s} \quad (4)$$

222 where  $[O_3]$  is the O<sub>3</sub> concentration at the reference level (nmol m<sup>-3</sup>),  $r_a$  is the  
223 aerodynamic and boundary layer resistance between leaf surface and reference level  
224 (s m<sup>-1</sup>).  $k_{O_3} = 1.67$  represents the ratio of leaf resistance for O<sub>3</sub> to that for water vapor.  
225  $r_s$  represents stomatal resistance (s m<sup>-1</sup>). For S2007 scheme, stomatal conductance is



226 damaged with the same ratio ( $1-F$ ) as photosynthesis and further affects  $O_3$  uptake.

227 As a comparison, the L2013 scheme applies separate  $O_3$  damaging relationships  
228 for photosynthetic rate and stomatal conductance. These independent relationships  
229 account for different plant groups and are calculated based on the cumulative uptake  
230 of  $O_3$  (CUO) under different levels of chronic  $O_3$  exposure. The leaf-level CUO  
231 ( $\text{mmol m}^{-2}$ ) over the growing season is calculated as follows:

$$232 \quad CUO = \sum (k_{O_3}/r_s + 1/r_a) \times [O_3]$$

233 (5)

234 The physical parameters in Equation (5) are the same as those in Equation (4).  $O_3$   
235 uptake is accumulated over time steps during the growing season with mean LAI >  
236 0.5 (Lombardozzi et al., 2012), when vegetation is most vulnerable to air pollution  
237 episodes.  $O_3$  uptake is only accumulated when  $O_3$  flux is above an instantaneous  
238 threshold of  $0.8 \text{ nmol } O_3 \text{ m}^{-2} \text{ s}^{-1}$  to account for ozone detoxification by vegetation at  
239 low  $O_3$  levels (Lombardozzi et al., 2015). We also include a leaf-turnover rate for  
240 evergreen plants so that the accumulation of  $O_3$  flux does not last beyond the average  
241 foliar lifetime. The  $O_3$  damaging ratios depend on CUO with empirical linear  
242 relationships as follows:

$$243 \quad F_{pO_3} = a_p \times CUO + b_p \quad (6)$$

$$244 \quad F_{cO_3} = a_c \times CUO + b_c \quad (7)$$

245 where  $F_{pO_3}$  and  $F_{cO_3}$  are the ozone damage ratios for photosynthesis and stomatal  
246 conductance, respectively. The slopes ( $a_p$  for photosynthesis and  $a_c$  for stomatal  
247 conductance) and intercepts ( $b_p$  for photosynthesis and  $b_c$  for stomatal conductance)  
248 of regression functions are determined based on the meta-analysis of hundreds of  
249 measurements (Table 2). The ratios predicted in Equations (6) and (7) are applied to  
250 photosynthesis and stomatal conductance, respectively, to account for their  
251 independent responses to  $O_3$  damages.

252

## 253 **2.4 Observational data**

254 We validated the simulated meteorology and air pollutants with observations.



255 The meteorological data were downloaded from the National Meteorological  
256 Information Center of China Meteorological Administration (CMA Meteorological  
257 Data Centre, 2022, <http://data.cma.cn/data/detail/dataCode/A.0012.0001.html>). The  
258 daily averaged surface pressure (PRES), wind speed at a height of 10 m (WS10),  
259 relative humidity (RH) and temperature at a height of 2 m (T2) were collected from  
260 839 ground stations. Hourly surface O<sub>3</sub> concentrations at 1597 sites in China were  
261 collected from Chinese National Environmental Monitoring Center (CNEMC,  
262 <http://websearch.mep.gov.cn/>).

263

## 264 **2.5. Simulations**

265 We performed seven experiments to quantify the damaging effects of ambient O<sub>3</sub>  
266 on GPP and the feedbacks to regional climate and air quality (Table 3). All  
267 simulations are conducted from 1<sup>st</sup> May to 31<sup>st</sup> August of 2017 with the first month  
268 excluded from the analysis as the spin-up. The control simulations (CTRL) excluded  
269 the impact of ozone on vegetation. Three offline simulations were performed with the  
270 same settings as the CTRL run, except that O<sub>3</sub> vegetation damages were calculated  
271 and output without feedback to affect vegetation growth. These offline runs were  
272 established using either the S2007 scheme (Offline\_SH07 for high sensitivity and  
273 Offline\_SL07 for low sensitivity) or the L2013 scheme (Offline\_L13). As a  
274 comparison, three online simulations applied the S2007 scheme (Online\_SH07 for  
275 high sensitivity and Online\_SL07 for low sensitivity) and the L2013 scheme  
276 (Online\_L13) to estimate the O<sub>3</sub> damages to GPP, which further influenced LAI  
277 development, leaf transpiration, and dry deposition. The differences between CTRL  
278 and Online runs indicated the responses of surface meteorology and O<sub>3</sub> concentrations  
279 to the O<sub>3</sub>-induced vegetation damages.

280

## 281 **3. Results**

### 282 **3.1 Model evaluations**

283 We compared the simulated summer near-surface temperature, relative humidity,



284 wind speed, and surface O<sub>3</sub> concentrations to observations. The model reasonably  
285 reproduces the spatial pattern of near-surface temperature with warmings in the  
286 Southeast and Northwest but coolings over the Tibetan Plateau (Figure 1a). On the  
287 national scale, the near-surface temperature is underestimated with a mean bias (MB)  
288 of 1.04 °C and a spatial R of 0.96. Unlike temperature, simulated relative humidity is  
289 overestimated with a MB of 5.04 % but a high R of 0.93 (Figure 1b). Due to the  
290 modeling biases in the topographic effects, simulated wind speed is overestimated by  
291 more than 1.06 m s<sup>-1</sup> on the national scale (Figure 1c). Such overestimation was also  
292 reported in other studies (Hu et al., 2016, Liu et al., 2020, Zhu et al., 2022).

293 Comparisons with the measurements from air quality sites show that the  
294 simulated O<sub>3</sub> deviates from the observed mean concentrations by 5.42 µg m<sup>-3</sup> with a  
295 spatial R of 0.68. The model reasonably captures the hotspots over North China Plain  
296 though with some overestimations. Such elevated bias in summer O<sub>3</sub> is a common  
297 issue for both global and regional models over Asia. For example, Zhu et al. (2022)  
298 overestimated summer average ozone concentration by 13.82 µg m<sup>-3</sup> in China. Liu et  
299 al. (2020) reached positive biases ranging from 3.7 µg m<sup>-3</sup> to 13.32 µg m<sup>-3</sup> using the  
300 WRF-CMAQ model. Overall, the WRF-Chem model shows reasonable performance  
301 in the simulation of surface meteorology and O<sub>3</sub> concentrations in China.

302

### 303 **3.2 Offline O<sub>3</sub> damage**

304 We compared the offline O<sub>3</sub> damage to photosynthesis between sunlit (PSNSUN)  
305 and shaded (PSNSHA) leaves during the summer. The S2007 scheme is dependent on  
306 instantaneous O<sub>3</sub> uptake, which peaks when both O<sub>3</sub> concentrations and stomatal  
307 conductance are high. For the same O<sub>3</sub> pollution level, the damages are much higher  
308 for the sunlit leaves (Figures 2a-2b) than that for the shaded leaves (Figures 2d-2e),  
309 because of the higher stomatal conductance linked with the more active  
310 photosynthesis for the sunlit leaves. In contrast, the L2013 scheme depends on the  
311 accumulated O<sub>3</sub> flux, which results in vegetation damage even at lower instant O<sub>3</sub>  
312 concentrations. As a result, we found limited differences in the O<sub>3</sub> damages between



313 sunlit (Figure 2c) and shaded (Figure 2f) leaves with L2013 scheme. Observations  
314 have reported that surface O<sub>3</sub> has limited impacts on the shaded leaves (Wan et al.,  
315 2014), consistent with the results simulated by the S2007 scheme. Furthermore,  
316 surface O<sub>3</sub> concentrations are low in southwest during summer (Figure 1d),  
317 suggesting a low O<sub>3</sub> vegetation damage over Tibetan Plateau and the more reasonable  
318 performance with the S2007 scheme.

319 Figure 3 shows the effect of O<sub>3</sub> damage to stomatal resistance of sunlit (RSSUN)  
320 and shaded (RSSHA) leaves. Overall, the spatial pattern of the changes in stomatal  
321 resistance is consistent with those of photosynthesis (Figure 2) but with opposite signs.  
322 Both RSSUN and RSSHA are enhanced by O<sub>3</sub> damage so as to prevent more O<sub>3</sub>  
323 uptake. For S2007 scheme, RSSUN with high and low sensitivities respectively  
324 increases by 13.43% (Figure 3a) and 8.35% (Figure 3b), higher than the rates of  
325 4.71% (Figure 3d) and 2.97% (Figure 3e) for RSSHA. These ratios are inversely  
326 connected to the changes of photosynthesis (Figure 2), suggesting the full coupling of  
327 damages between leaf photosynthesis and stomatal conductance. For L2013 scheme,  
328 predicted changes in RSSUN (Figure 3c) and RSSHA (Figure 3f) are very similar  
329 with the magnitude of 25.3%-26.3%. These changes are higher than the loss of  
330 photosynthesis (Figures 2c and 2f), suggesting the decoupling of O<sub>3</sub> damages to leaf  
331 photosynthesis and stomatal conductance as revealed by the L2013 scheme.

332 We further assessed the O<sub>3</sub> damage to GPP and transpiration (TR). For S2007  
333 scheme, O<sub>3</sub> causes damages to GPP and TR approximately by 5.5% with low  
334 sensitivity (Figures 4b and 4e) and 8.4% with high sensitivity (Figures 4a and 4d)  
335 compared to the CTRL simulation. The model predicts high GPP damages over North  
336 China Plain and moderate damages in the southeastern and northeastern regions. In  
337 the northwest, GPP damage is very limited due to the low relative humidity (Figure 1b)  
338 that constrains the stomatal uptake. For L2013 scheme, TR shows uniform reductions  
339 exceeding -25% in most regions of China except for the northwest (Figure 4f), though  
340 O<sub>3</sub> concentrations show distinct spatial gradient (Figure 1d). The changes of GPP are  
341 similar to that of TR but with lower inhibitions (Figure 4c). On average, the GPP



342 reduction with the L2013 scheme is 2.5-3.9 times of that predicted with the S2007  
343 scheme. The most significant differences are located in Tibetan Plateau with limited  
344 damages in S2007 but strong inhibitions in L2013. Given the cold environment  
345 (Figure 1a) that constrains stomatal uptake (Wilkinson et al., 2001), we consider the  
346 low O<sub>3</sub> impacts in Tibetan Plateau predicted with S2007 scheme are more reasonable.

347

### 348 **3.3 The O<sub>3</sub>-vegetation feedback to surface energy and meteorology**

349 The O<sub>3</sub> vegetation damage causes contrasting responses in surface sensible heat  
350 (SH) and LH (Figure 5). For S2007 scheme, the SH fluxes on average increase by  
351 3.17 W m<sup>-2</sup> (8.85%) with low sensitivity (Figure 5b) and 5.99 W m<sup>-2</sup> (16.22%) with  
352 high sensitivity (Figure 5a). The maximum enhancement is located in southern China,  
353 where the increased stomatal resistance (Figure 3a) reduces transpiration and the  
354 consequent heat dissipation. Meanwhile, LH fluxes decrease by 3.26 W m<sup>-2</sup> (5.58%)  
355 with low sensitivity (Figure 5e) and 6.43 W m<sup>-2</sup> (15.29%) with high sensitivity  
356 (Figure 5d), following the reductions in transpiration (Figures 4d and 4e). We found  
357 similar changes in surface energy by O<sub>3</sub>-vegetation coupling between the S2007 and  
358 L2013 schemes. The SH shows the same hotspots over southern China with national  
359 average increase of 12.85% (Figure 5c), which is within the range of 8.85% to  
360 16.22% predicted by the S2007 scheme. The LH largely decreases in central and  
361 northern China with the mean reduction of 17.4% (Figure 5f), close to the magnitude  
362 of 15.29% predicted with the S2007 scheme using the high O<sub>3</sub> sensitivity (Figure 5d).  
363 Although the offline damages to GPP and TR are much larger with the L2013 than  
364 S2007 (Figure 4), their feedback to surface energy shows consistent spatial pattern  
365 and magnitude (Figure 5), likely because the O<sub>3</sub> inhibition in S2007 has the same  
366 diurnal cycle with energy fluxes while the L2013 scheme shows almost constant  
367 inhibitions through the day (Figure S1). The nighttime damages in L2013 have  
368 limited contributions to the changes of surface energy, which usually peaks at the  
369 daytime.

370 The O<sub>3</sub>-induced damages to stomatal conductance weaken plant transpiration and



371 thus slow down the heat dissipation at the surface, leading to the higher temperature  
372 but lower RH in China (Figure 6). On the national scale, temperature increases by  
373 0.5 °C due to O<sub>3</sub> vegetation damage with the high sensitivity (Figure 6a) and 0.23 °C  
374 with the low sensitivity (Figure 6b) predicted using the S2007 scheme. A similar  
375 warming is predicted with the L2013 scheme except that temperature shows moderate  
376 enhancement over Tibetan Plateau (Figure 6c). The average RH decreases by 3.68%  
377 with the high O<sub>3</sub> sensitivity (Figure 6d) and 2.22% with the low sensitivity (Figure 6e)  
378 in response to the suppressed plant transpiration. A stronger RH reduction of -3.85%  
379 is achieved with the L2013 scheme, which predicts the maximum RH reductions in  
380 the North (Figure 6f).

381

### 382 **3.4 The O<sub>3</sub>-vegetation feedback to air quality**

383 The O<sub>3</sub>-induced inhibition on stomatal resistance leads to a significant increase  
384 in surface O<sub>3</sub> concentrations, particularly in eastern China (Figures 7a-7c). The main  
385 cause of such feedback is the reduction in O<sub>3</sub> dry deposition, which exacerbates the O<sub>3</sub>  
386 pollution in China. For S2007 scheme, this positive feedback can reach up to 15 µg  
387 m<sup>-3</sup> with high sensitivity (Figure 7a) and 8 µg m<sup>-3</sup> with low sensitivity (Figure 7b)  
388 over North China Plain. On the national scale, surface O<sub>3</sub> enhances 3.31 µg m<sup>-3</sup> (1.25  
389 µg m<sup>-3</sup>) or 7.92 µg m<sup>-3</sup> (3.04%) with the high (low) O<sub>3</sub> sensitivity. For L2013 scheme,  
390 the changes of O<sub>3</sub> concentration (Figure 7c) are comparable to that of the S2007  
391 scheme with high sensitivity (Figure 7a), except that the O<sub>3</sub> enhancement is stronger  
392 in the Southeast but weaker in the Northeast.

393 The O<sub>3</sub>-vegetation coupling also increases surface isoprene emissions. For S2007  
394 scheme, isoprene emissions increase by 6.13% with high sensitivity (Figure 7d) and  
395 3.43% with low sensitivity (Figure 7e), with regional hotspots in North China Plain,  
396 northeastern and southern regions. The predictions using L2013 scheme (Figure 7f)  
397 show very similar patterns and magnitude of isoprene changes to the S2007 scheme  
398 with high sensitivity. Such enhancement in isoprene emissions is related to the  
399 additional surface warming by O<sub>3</sub>-vegetation interactions (Figures 6a-6c). In turn, the



400 increased isoprene emissions contribute to the deterioration of O<sub>3</sub> pollution in China.

401

#### 402 **4. Conclusions and discussion**

403 In this study, we explored the feedback of O<sub>3</sub>-vegetation coupling to surface  
404 meteorology and air quality in China using two O<sub>3</sub> damage schemes embedded in a  
405 regional meteorology-chemistry coupled model. The two schemes predicted distinct  
406 spatial patterns with much larger magnitude of GPP loss in the L2013 scheme than  
407 that in the S2007 scheme. We further distinguished the leaf responses with different  
408 illuminations. For the S2007 scheme, the damages to photosynthesis of sunlit leaves  
409 are ~2.6 times of that to shaded leaves. However, for the L2013 scheme, limited  
410 differences are found between the sunlit and shaded leaves. The damages to leaf  
411 photosynthesis increase stomatal resistance, leading to the reductions of transpiration  
412 but enhancement of sensible heat due to the less efficient heat dissipation. These  
413 changes in surface energy and water fluxes feed back to increase surface temperature  
414 but decrease relative humidity. Although the L2013 scheme predicts much stronger  
415 offline damages, the feedback causes very similar pattern and magnitude in surface  
416 warming as the S2007 scheme. Consequently, surface O<sub>3</sub> increases due to the stomatal  
417 closure and isoprene emissions enhance due to the anomalous warming.

418 Our predicted O<sub>3</sub> damage to GPP was within the range of -4% to -40% as  
419 estimated in previous studies using different models and/or parameterizations over  
420 China (Ren et al., 2011; Lombardozzi et al., 2015; Yue et al., 2015; Sadiq et al., 2017;  
421 Xie et al., 2019; Zhu et al., 2022; Jin et al., 2023). Such a wide span revealed the large  
422 uncertainties in the estimate of O<sub>3</sub> impacts on ecosystem functions. In this study, we  
423 employed two schemes and compared their differences. With the S2007 scheme, we  
424 predicted GPP reductions of -5.5% to -8.5% in China, similar to the range of -4% to  
425 -10% estimated by Yue et al. (2015) using the same O<sub>3</sub> damage scheme but lower than  
426 the estimate of -12.1% predicted by Xie et al. (2019), likely due to the slight  
427 overestimation of surface O<sub>3</sub> in the latter study. With the L2013 scheme, we predicted  
428 much larger GPP reductions of -21.4%. However, such value was still lower than the



429 -28.9% in Jin et al. (2023) and -20% to -40% in Zhu et al. (2022) using the same  
430 L2013 scheme embedded in WRF-Chem model, though all studies showed similar  
431 spatial patterns in the GPP reductions. Such differences were likely attributed to the  
432 varied model configuration as we ran the model from May while the other studies  
433 started from the beginning of years. The longer time for the accumulation of O<sub>3</sub>  
434 stomatal uptake in other studies resulted in higher damages than our estimates with  
435 the L2013 scheme.

436 The O<sub>3</sub>-vegetation coupling caused strong feedback to surface meteorology and  
437 air quality. Our simulations with either scheme revealed that surface SH increases by  
438 2-28 W m<sup>-2</sup> and LH decreases by 4-32 W m<sup>-2</sup> over eastern China, consistent with the  
439 estimates of 5-30 W m<sup>-2</sup> by Zhu et al. (2022) using WRF-Chem model with the L2013  
440 scheme. Consequently, surface air temperature on average increases by 0.23-0.51°C  
441 while relative humidity decreases by 2.2-3.8%, similar to the warming of 0.2-0.8°C  
442 and RH reduction of 3% as predicted by Zhu et al. (2022). However, these changes in  
443 surface energy flux and meteorology are much higher than that in Jin et al. (2023),  
444 likely because the latter focuses on the perturbations averaged throughout the year  
445 instead of summer period as in this study and Zhu et al. (2022). We further predicted  
446 that O<sub>3</sub> vegetation damage increased surface O<sub>3</sub> by 0.6-1.7 ppbv in China, similar to  
447 the 1.2-2.1 ppbv estimated for eastern China using a global model (Gong et al., 2020).  
448 Regionally, the O<sub>3</sub> enhancement reached as high as 4-7.5 ppbv in North China Plain,  
449 consistent with the maximum value of 6 ppbv over the same domain predicted by Zhu  
450 et al. (2022). However, limited feedback to surface O<sub>3</sub> was predicted in Jin et al.  
451 (2023), mainly because the decreased dry deposition had comparable but opposite  
452 effects to the decreased isoprene emissions due to the reductions of LAI. Such  
453 discrepancy was likely caused by the stronger O<sub>3</sub> inhibition in Jin et al. (2023)  
454 following the longer period of O<sub>3</sub> accumulation, consequently exacerbating the  
455 negative impacts of LAI reductions on O<sub>3</sub> production.

456 There were some limitations in our parameterizations and simulations. The  
457 WRF-Chem model slightly overestimated summer O<sub>3</sub> concentrations, which could



458 exacerbate the damages to stomatal conductance and the subsequent feedback. The  
459 S2007 scheme employed the coupled responses in photosynthesis and stomatal  
460 conductance to O<sub>3</sub> vegetation damage. However, some observations revealed that  
461 stomatal response is slow under long-term O<sub>3</sub> exposure, resulting in loss of stomatal  
462 function and decoupling from photosynthesis (Calatayud et al., 2007; Lombardozzi et  
463 al., 2012). The L2013 scheme considered the decoupling between photosynthesis and  
464 stomatal conductance. However, this scheme could not distinguish the responses of  
465 sunlit and shaded leaves. In addition, the calculation of CUO heavily relied on the  
466 ozone threshold and accumulation period, leading to varied responses among different  
467 studies using the same scheme. Furthermore, the slopes of O<sub>3</sub> sensitivity in L2013  
468 scheme were set to zero for some PFTs, leading to constant damages independent of  
469 CUO. Finally, the current knowledge of the O<sub>3</sub> effects on stomatal conductance was  
470 primarily derived from leaf-level measurements (Matyssek et al., 2008), which were  
471 much fewer compared to that for photosynthesis. The limited data availability and  
472 lack of inter-PFT responses constrain the development of empirical parameterizations.

473 Despite these limitations, our study provided the first comparison of different  
474 parameterizations in simulating O<sub>3</sub>-vegetation interactions. We found similar  
475 feedbacks to surface energy and meteorology though the two schemes showed varied  
476 magnitude and distribution in the offline responses of GPP and stomatal conductance  
477 to surface O<sub>3</sub>. The main cause of such inconsistency lied in the low feedback of  
478 damages in L2013 with some unrealistic inhibitions of ecosystem functions at night  
479 and over the regions with low O<sub>3</sub> level. Such similarity provides a solid foundation for  
480 the exploration of O<sub>3</sub>-vegetation coupling using different schemes. The positive  
481 feedback of O<sub>3</sub> vegetation damage to surface air temperature and O<sub>3</sub> concentrations  
482 posed emerging but ignored threats to both climate change and air quality in China.

483

#### 484 **Data availability**

485 The observed hourly O<sub>3</sub> concentrations were obtained from Chinese National  
486 Environmental Monitoring Center (CNEMC, <http://websearch.mep.gov.cn/>). The



487 observed meteorological data were obtained from the National Meteorological  
488 Information Center of China Meteorological Administration (CMA Meteorological  
489 Data Centre, 2022, <http://data.cma.cn/data/detail/dataCode/A.0012.0001.html>). The  
490 MEIC and MIX emission inventory are available at  
491 ([http://meicmodel.org.cn/?page\\_id=560](http://meicmodel.org.cn/?page_id=560) and [http://meicmodel.org.cn/?page\\_id=89](http://meicmodel.org.cn/?page_id=89)).

492

#### 493 **Author contributions**

494 XY conceived the study. XY and JC designed the research and carried out the  
495 simulations. JC completed data analysis and the first draft. MM provided useful  
496 comments on the paper. XY reviewed and edited the manuscript.

497

#### 498 **Competing interests**

499 The authors declare that they have no conflict of interest.

500

#### 501 **Acknowledgments**

502 This study was jointly funded by the National Natural Science Foundation of  
503 China (grant no. 42293323) and Jiangsu Funding Program for Excellent Postdoctoral  
504 Talent (2023ZB737).

505

#### 506 **References**

- 507 Ainsworth, E. A., Yendrek, C. R., Sitch, S., Collins, W. J., and Emberson, L. D.: The  
508 effects of tropospheric ozone on net primary productivity and implications for  
509 climate change, *Annu. Rev. Plant Biol.*, 63, 637–661,  
510 <https://doi.org/10.1146/annurevarplant-042110-103829>, 2012.
- 511 Ball, J. T., Woodrow, I. E., and Berry, J. A.: A model predicting stomatal conductance  
512 and its contribution to the control of photosynthesis under different  
513 environmental conditions, *Prog. Photosynthesis*, Springer, Dordrecht, 4, 221–224,  
514 1987.
- 515 Calatayud, V., Cerveró, J., and Sanz, M. J.: Foliar, physiological and growth responses  
516 of four maple species exposed to ozone, *Water Air Soil Pollut.*, 185, 239–254,



- 517 <https://doi.org/10.1007/s11270-007-9446-5>, 2007.
- 518 Chou, M.-D. and Suarez, M.J.: An Efficient Thermal Infrared Radiation  
519 Parameterization for Use in General Circulation Models. Technical Report, 85p.  
520 1994.
- 521 Dickinson, R. E.: Land surface processes and climate – Surface albedos and energy  
522 balance, *Adv. Geophys.*, 25, 305–353,  
523 [https://doi.org/10.1016/S0065-2687\(08\)60176-4](https://doi.org/10.1016/S0065-2687(08)60176-4), 1983.
- 524 Emmons, L. K., Walters, S., Hess, P. G., Lamarque, J.-F., Pfister, G. G., Fillmore, D.,  
525 Granier, C., Guenther, A., Kinnison, D., Laepple, T., Orlando, J., Tie, X., Tyndall,  
526 G., Wiedinmyer, C., Baughcum, S. L., and Kloster, S.: Description and  
527 evaluation of the Model for Ozone and Related chemical Tracers, version 4  
528 (MOZART-4), *Geosci. Model Dev.*, 3, 43–67,  
529 <https://doi.org/10.5194/gmd-3-43-2010>, 2010.
- 530 Farquhar, G. D., Caemmerer, S. V., and Berry, J. A.: A biochemical model of  
531 photosynthetic CO<sub>2</sub> assimilation in leaves of C<sub>3</sub> species, *Planta*, 149, 78–90,  
532 <https://doi.org/10.1007/bf00386231>, 1980.
- 533 Felzer, B., Kicklighter, D., Melillo, J., Wang, C., Zhuang, Q., and Prinn, R.: Effects of  
534 ozone on net primary production and carbon sequestration in the conterminous  
535 United States using a biogeochemistry model, *Tellus B*, 56, 230–248,  
536 <https://doi.org/10.1111/j.1600-0889.2004.00097.x>, 2004.
- 537 Feng, Z., Hu, E., Wang, X., Jiang, L., and Liu, X.: Ground-level O<sub>3</sub> pollution and its  
538 impacts on food crops in China: A review, *Environ. Pollut.*, 199, 42–48,  
539 <https://doi.org/10.1016/j.envpol.2015.01.016>, 2015.
- 540 Gong, C., Lei, Y., Ma, Y., Yue, X., and Liao, H.: Ozone–vegetation feedback through  
541 dry deposition and isoprene emissions in a global chemistry–carbon–climate  
542 model, *Atmos. Chem. Phys.*, 20, 3841–3857,  
543 <https://doi.org/10.5194/acp-203841-2020>, 2020.
- 544 Gong, C., Yue, X., Liao, H., and Ma, Y.: A humidity-based exposure index  
545 representing ozone damage effects on vegetation, *Environ. Res. Lett.*, 16, 044030,



- 546 <https://doi.org/10.1088/1748-9326/abecbb>, 2021.
- 547 Grell, G. A., McKeen, S., Michalakes, J., Bao, J.-W., Trainer, M., and Hsie, E.-Y.:  
548 Real-time simultaneous prediction of air pollution and weather during the  
549 Houston 2000 Field Experiment, presented at the 4th Conference on  
550 Atmospheric Chemistry: Atmospheric Chemistry and Texas Field Study, 13–17  
551 January, American Meteorological Society, Orlando, 2002.
- 552 Grell, G. A., Peckham, S. E., Schmitz, R., McKeen, S. A., Frost, G., Skamarock, W.  
553 C., and Eder, B.: Fully coupled “online” chemistry within the WRF model.  
554 *Atmos. Environ.*, 39, 6957–6975,  
555 <https://doi.org/10.1016/j.atmosenv.2005.04.027>, 2005.
- 556 Guenther, A., Karl, T., Harley, P., Wiedinmyer, C., Palmer, P. I., and Geron, C.:  
557 Estimates of global terrestrial isoprene emissions using MEGAN (Model of  
558 Emissions of Gases and Aerosols from Nature), *Atmos. Chem. Phys.*, 6,  
559 3181–3210, <https://doi.org/10.5194/acp-6-3181-2006>, 2006.
- 560 Hersbach, H., Bell, B., Berrisford, P., Hirahara, S., Horányi, A., Muñoz-Sabater, J.,  
561 Nicolas, J., Peubey, C., Radu, R., Schepers, D., Simmons, A., Soci, C., Abdalla,  
562 S., Abellan, X., Balsamo, G., Bechtold, P., Biavati, G., Bidlot, J., Bonavita, M.,  
563 De Chiara, G., Dahlgren, P., Dee, D., Diamantakis, M., Dragani, R., Flemming,  
564 J., Forbes, R., Fuentes, M., Geer, A., Haimberger, L., Healy, S., Hogan, R. J.,  
565 Hólm, E., Janisková, M., Keeley, S., Laloyaux, P., Lopez, P., Lupu, C., Radnoti,  
566 G., de Rosnay, P., Rozum, I., Vamborg, F., Villaume, S., and Thépaut, J.-N.: The  
567 ERA5 global reanalysis, *Q. J. Roy. Meteor. Soc.*, 146, 1999–2049, 2020.
- 568 Hong, S.-Y., Noh, Y., and Dudhia, J.: A new vertical diffusion package with explicit  
569 treatment of entrainment processes, *Mon. Weather Rev.*, 134, 2318–2341,  
570 <https://doi.org/10.1175/MWR3199.1>, 2006.
- 571 Hu, J., Chen, J., Ying, Q., and Zhang, H.: One-year simulation of ozone and  
572 particulate matter in China using WRF/CMAQ modeling system, *Atmos. Chem.*  
573 *Phys.*, 16, 10333–10350, <https://doi.org/10.5194/acp-16-10333-2016>, 2016.
- 574 Jin, Z., Yan, D., Zhang, Z., Li, M., Wang, T., Huang, X., Xie, M., Li S and Zhuang.:



- 575 Effects of elevated ozone exposure on regional meteorology and air quality in  
576 China through ozone-vegetation coupling. *J. Geophys. Res.-Atmos.*, 128,  
577 e2022JD038119. <https://doi.org/10.1029/2022JD038119>, 2023.
- 578 Li, J., Mahalov, A., and Hyde, P.: Simulating the impacts of chronic ozone exposure  
579 on plant conductance and photosynthesis, and on the regional hydroclimate using  
580 WRF/Chem, *Environ. Res. Lett.*, 11, 114017,  
581 <https://doi.org/10.1088/17489326/11/11/114017>, 2016.
- 582 Li, P., Calatayud, V., Gao, F., Uddling, J., and Feng, Z. Z.: Differences in ozone  
583 sensitivity among woody species are related to leaf morphology and antioxidant  
584 levels, *Tree Physiol.*, 36, 1105– 1116, <https://doi.org/10.1093/treephys/tpw042>,  
585 2016.
- 586 Li, P., Feng, Z., Catalayud, V., Yuan, X., Xu, Y., and Paoletti, E.: A meta-analysis on  
587 growth, physiological, and biochemical responses of woody species to  
588 ground-level ozone highlights the role of plant functional types, *Plant Cell*  
589 *Environ.*, 40, 2369–2380, <https://doi.org/10.1111/pce.13043>, 2017.
- 590 Liu, Y. and Wang, T.: Worsening urban ozone pollution in China from 2013 to 2017 –  
591 Part 1: The complex and varying roles of meteorology, *Atmos. Chem. Phys.*, 20,  
592 6305–6321, <https://doi.org/10.5194/acp-20-6305-2020>, 2020.
- 593 Lombardozi, D., Levis, S., Bonan, G., and Sparks, J. P.: Predicting photosynthesis  
594 and transpiration responses to ozone: decoupling modeled photosynthesis and  
595 stomatal conductance, *Biogeosciences*, 9, 3113–3130,  
596 <https://doi.org/10.5194/bg-9-31132012>, 2012.
- 597 Lombardozi, D., Sparks, J. P., and Bonan, G.: Integrating O<sub>3</sub> influences on terrestrial  
598 processes: photosynthetic and stomatal response data available for regional and  
599 global modeling, *Biogeosciences*, 10, 6815–6831,  
600 <https://doi:10.5194/bg-10-6815-2013>, 2013.
- 601 Lombardozi, D., Levis, S., Bonan, G., Hess, P. G., and Sparks, J. P.: The influence of  
602 chronic ozone exposure on global carbon and water cycles, *J. Climate*, 28,  
603 292–305, <https://doi.org/10.1175/JCLI-D-14-00223.1>, 2015.



- 604 Matyssek, R., Sandermann, H., Wieser, G., Booker, F., Cieslik, S., Musselman, R.,  
605 and Ernst, D.: The challenge of making ozone risk assessment for forest trees  
606 more mechanistic, *Environ. Pollut.*, 156, 567–582,  
607 <https://doi.org/10.1016/j.envpol.2008.04.017>, 2008.
- 608 Mlawer, E. J., Taubman, S. J., Brown, P. D., Iacono, M. J., and Clough, S. A.:  
609 Radiative transfer for inhomogeneous atmosphere: RRTM, a validated  
610 correlated-k model for the longwave, *J. Geophys. Res-Atmos.*, 102(D14), 16  
611 663–16 682, <https://doi.org/10.1029/97JD00237>, 1997.
- 612 Monks, P. S., Archibald, A. T., Colette, A., Cooper, O., Coyle, M., Derwent, R.,  
613 Fowler, D., Granier, C., Law, K. S., Mills, G. E., Stevenson, D. S., Tarasova, O.,  
614 Thouret, V., von Schneidmesser, E., Sommariva, R., Wild, O., and Williams, M.  
615 L.: Tropospheric ozone and its precursors from the urban to the global scale from  
616 air quality to short-lived climate forcer, *Atmos. Chem. Phys.*, 15, 8889–8973,  
617 <https://doi.org/10.5194/acp-15-8889-2015>, 2015.
- 618 Morrison, H., Thompson, G., and Tatarskii, V.: Impact of cloud microphysics on the  
619 development of trailing stratiform precipitation in a simulated squall line:  
620 comparison of one- and two-moment schemes, *Monthly Weather Review*, 137,  
621 991–1007, <https://doi.org/10.1175/2008MWR2556.1>, 2009.
- 622 Niu, G. Y., Yang, Z. L., Mitchell, K. E., Chen, F., Ek, M. B., Barlage, M., Kumar, A.,  
623 Manning, K., Niyogi, D., Rosero, E., Tewari, M., and Xia, Y.: The community  
624 Noah land surface model with multiparameterization options (Noah-MP): 1.  
625 Model description and evaluation with local-scale measurements, *J. Geophys.*  
626 *Res-Atmos.*, 116, D12, <https://doi.org/10.1029/2010JD015139>, 2011.
- 627 Ren, W., Tian, H., Tao, B., Chappelka, A., Sun, G., Lu, C., Liu, M., Chen, G., and Xu,  
628 X.: Impacts of tropospheric ozone and climate change on net primary  
629 productivity and net carbon exchange of China's forest ecosystems, *Glob. Ecol.*  
630 *Biogeogr.*, 20, 391–406, <https://doi.org/10.1111/j.1466-8238.2010.00606.x>, 2011.
- 631 Sadiq, M., Tai, A. P. K., Lombardozzi, D., and Val Martin, M.: Effects of  
632 ozone–vegetation coupling on surface ozone air quality via biogeochemical and



- 633 meteorological feedbacks, *Atmos. Chem. Phys.*, 17, 3055–3066,  
634 <https://doi.org/10.5194/acp-17-3055-2017>, 2017.
- 635 Sitch, S., Cox, P. M., Collins, W. J., and Huntingford, C.: Indirect radiative forcing of  
636 climate change through ozone effects on the land-carbon sink, *Nature*, 448,  
637 791–794, <https://doi.org/10.1038/nature06059>, 2007.
- 638 Skamarock W C and Klemp J B. A time-split nonhydrostatic atmospheric model for  
639 weather research and forecasting applications. *J. Comput. Phys.*, 227(7):  
640 3465-3485, <https://doi.org/10.1016/j.jcp.2007.01.037>, 2008.
- 641 Su, B., Zhou, M., Xu, H., Zhang, X., Li, Y., Su, H., and Xiang B.: Photosynthesis and  
642 biochemical responses to elevated O<sub>3</sub> in *Plantago major* and *Sonchus oleraceus*  
643 growing in a lowland habitat of northern China, *J. Environ. SCI.*, 53(3): 113-121,  
644 <https://doi.org/10.1016/j.jes.2016.05.011>, 2017.
- 645 Tie, X. X., Madronich, S., Walters, S., Zhang, R. Y., Rasch, P., and Collins, W.: Effect  
646 of clouds on photolysis and oxidants in the troposphere, *J. Geophys. Res.-Atmos.*,  
647 108, 4642, <https://doi.org/10.1029/2003jd003659>, 2003.
- 648 Wan, W., Manning, WJ., Wang, X., Zhang, H., Sun, X., and Zhang, Q.: Ozone and  
649 ozone injury on plants in and around Beijing, China, *Environ Pollut.*, 191:  
650 215-222, <https://doi.org/10.1016/j.envpol.2014.02.035>, 2014
- 651 Wilkinson, S., Clephan, A. L., and Davies, W. J.: Rapid Low Temperature-Induced  
652 Stomatal Closure Occurs in Cold-Tolerant *Commelina Communis* Leaves But  
653 Not in Cold-Sensitive Tobacco Leaves, via a Mechanism That Involves  
654 Apoplastic Calcium But Not Abscisic Acid. *Plant Physiol.*, 126, 1566–1578.  
655 <https://doi.org/10.1104/pp.126.4.1566>, 2001.
- 656 Wittig, V. E., Ainsworth, E. A., and Long, S. P.: To what extent do current and  
657 projected increases in surface ozone affect photosynthesis and stomatal  
658 conductance of trees? A metaanalytic review of the last 3 decades of experiments,  
659 *Plant Cell Environ.*, 30, 1150–1162,  
660 <https://doi.org/10.1111/j.13653040.2007.01717.x>, 2007.
- 661 Xie, X., Wang, T., Yue, X., Li, S., Zhuang, B., Wang, M., and Yang, X.: Numerical



662 modeling of ozone damage to plants and its effects on atmospheric CO<sub>2</sub> in China,  
663 Atmos. Environ., 217, 116970, <https://doi.org/10.1016/j.atmosenv.2019.116970>,  
664 2019.

665 Yue, X. and Unger, N.: Ozone vegetation damage effects on gross primary  
666 productivity in the United States, Atmos. Chem. Phys., 14, 9137–9153,  
667 <https://doi.org/10.5194/acp-14-9137-2014>, 2014.

668 Yue, X. and Unger, N.: The Yale Interactive terrestrial Biosphere model version 1.0:  
669 description, evaluation and implementation into NASA GISS ModelE2, Geosci.  
670 Model Dev., 8, 2399–2417, <https://doi.org/10.5194/gmd-8-2399-2015>, 2015.

671 Zaveri, R. A., and Peters, L. K.: A new lumped structure photochemical mechanism  
672 for large-scale applications, J Geophys Res-Atmos, 104, 30387-30415, 1999.

673 Zaveri, R. A., Easter, R. C., Fast, J. D., and Peters, L. K.: Model for simulating  
674 aerosol interactions and chemistry (MOSAIC), J. Geophys. Res-Atmos., 113,  
675 D13204, <https://doi.org/10.1029/2007JD008782>, 2008.

676 Zhou, S. S., Tai, A. P. K., Sun, S., Sadiq, M., Heald, C. L., and Geddes, J. A.:  
677 Coupling between surface ozone and leaf area index in a chemical transport  
678 model: strength of feedback and implications for ozone air quality and vegetation  
679 health, Atmos. Chem. Phys., 18, 14133–14148,  
680 <https://doi.org/10.5194/acp-18-14133-2018>, 2018.

681 Zhu, J., Tai, A. P. K., and Yim, S. H. L.: Effects of ozone-vegetation interactions on  
682 meteorology and air quality in China using a two-way coupled land-atmosphere  
683 model, Atmos. Chem. Phys., 22, 765-782,  
684 <https://doi.org/10.5194/acp-22-765-2022>, 2022.  
685



686 **Tables**

687

**Table 1.** Parameters used for S2007 O<sub>3</sub> damage scheme.

PFTs <sup>a</sup>	$a_{PFT}$ (nmol <sup>-1</sup> m <sup>2</sup> s) <sup>b</sup>	$\gamma_{PFT}$ (nmol m <sup>-2</sup> s <sup>-1</sup> )
EBF	0.075, 0.02	1.6
NF	0.075, 0.02	1.6
DBF	0.15, 0.04	1.6
SHR	0.1, 0.03	1.6
GRA	1.4, 0.25	5
CRO	1.4, 0.25	5

688 <sup>a</sup> The plant functional types (PFTs) include evergreen broadleaf forest (EBF),  
689 needleleaf forest (NF), deciduous broadleaf forest (DBF), shrubland (SHR), grassland  
690 (GRA), and cropland (CRO).

691 <sup>b</sup> The first number is for high sensitivity and the second is for low sensitivity.

692



693

694 **Table 2.** Slopes and intercepts used for L2013 O<sub>3</sub> damage scheme.

PFTs	$a_p$ (mmol m <sup>-2</sup> )	$b_p$	$a_c$ (mmol m <sup>-2</sup> )	$b_c$
EBF	0	0.8752	0	0.9125
NF	0	0.839	0.0048	0.7823
DBF	0	0.8752	0	0.9125
SHR	0	0.8752	0	0.9125
GRA	-0.0009	0.8021	0	0.7511
CRO	-0.0009	0.8021	0	0.7511

695

696

697



698

**Table 3.** Summary of simulation experiments

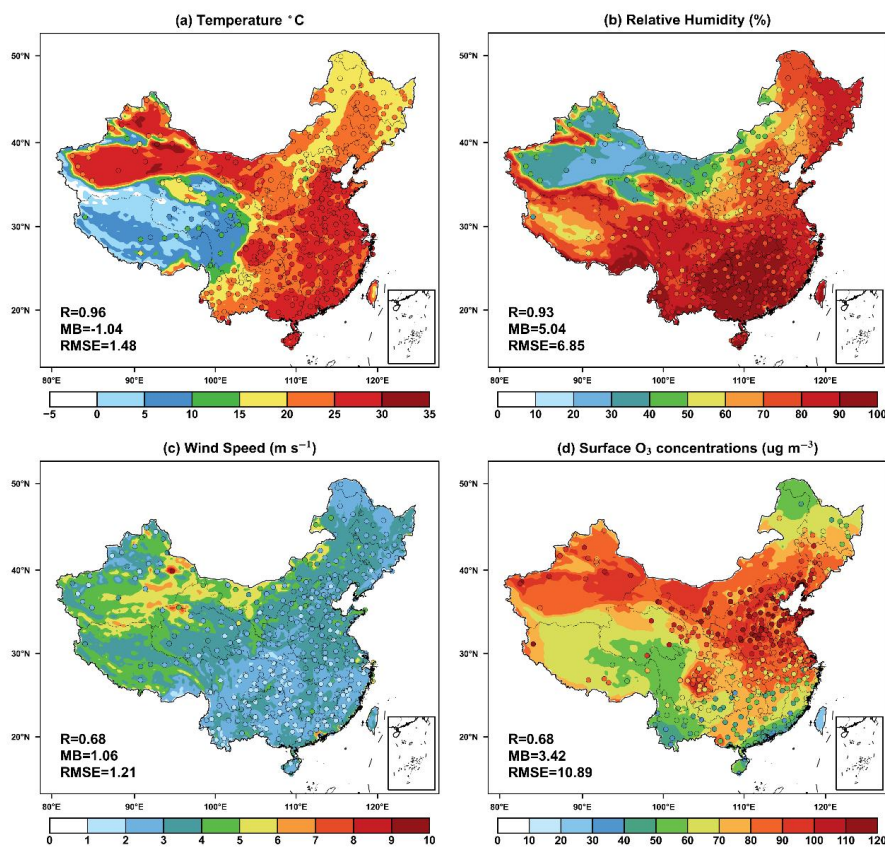
Name	O <sub>3</sub> damage to vegetable	Scheme
CRTL	-	-
Offline_SH07	High	Sitch et al. (2007)
Offline_SL07	Low	Sitch et al. (2007)
Offline_L13	-	Lombardozzi et al. (2013)
Online_SH07	High	Sitch et al. (2007)
Online_SL07	Low	Sitch et al. (2007)
Online_L13	-	Lombardozzi et al. (2013)

699

700



701 **Figure captions**



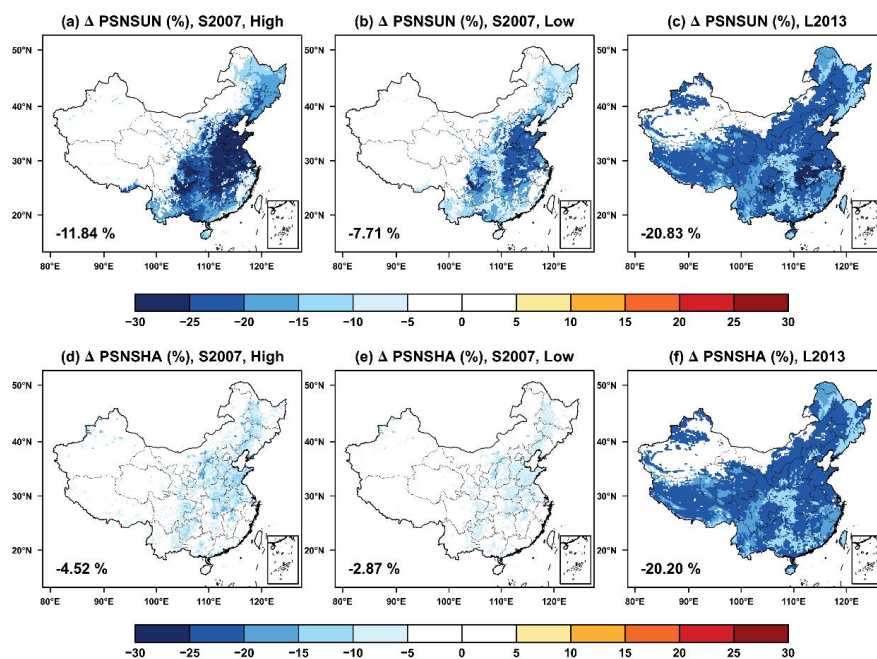
702

703

704

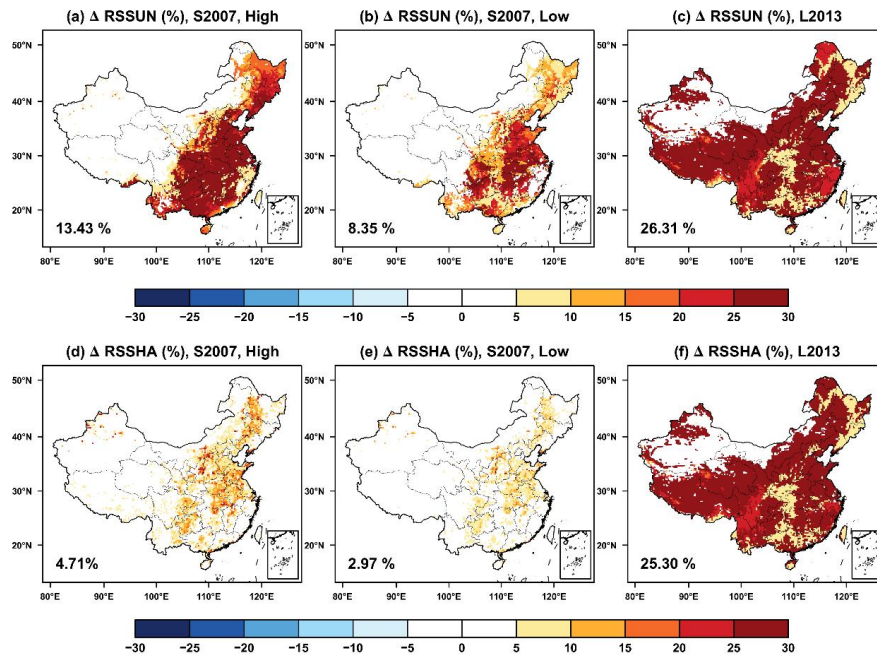
705 **Figure 1** Evaluations of simulated summer (June–August) daily (24-h average) (a)  
706 near-surface temperature, (b) relative humidity, (c) wind speed, and (d) surface O<sub>3</sub>  
707 concentrations in China. The dots represent the site-level observations. The  
708 correlation coefficients (R), mean biases (MB), and root-mean-square error (RMSE)  
709 for the comparisons are shown in the lower left corner of each panel.

710



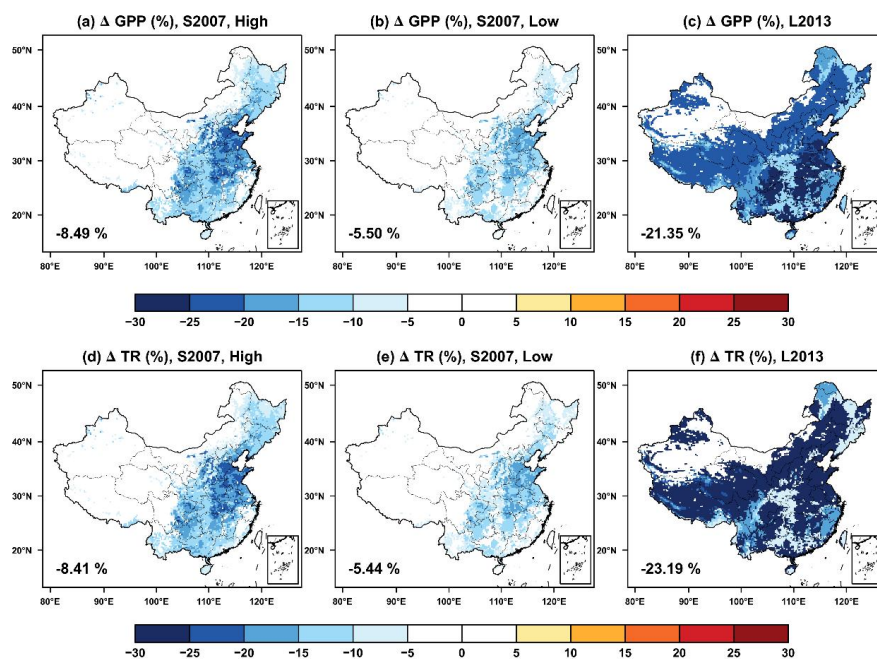
711  
712  
713  
714  
715  
716  
717  
718

**Figure 2** Offline O<sub>3</sub> damage (%) to the summertime photosynthesis of (a-c) sunlit and (d-f) shaded leaves predicted by the S2007 scheme with (a, d) high and (b, e) low sensitivities or the (c, f) L2013 scheme. The area-weighted percentage changes are shown in the lower left corner.



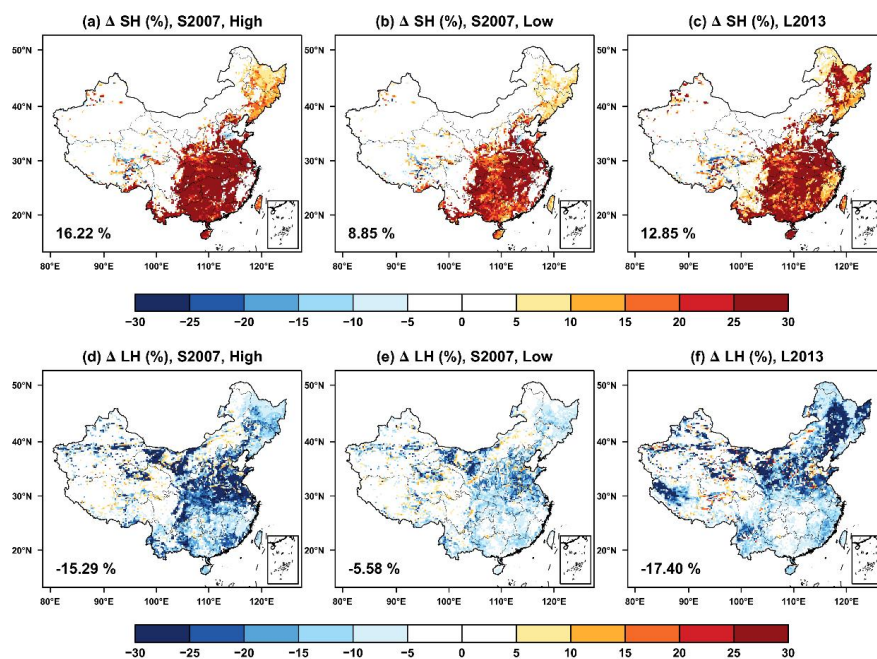
719  
720  
721  
722  
723

**Figure 3** The same as Figure 2 but for the changes in stomatal resistance.



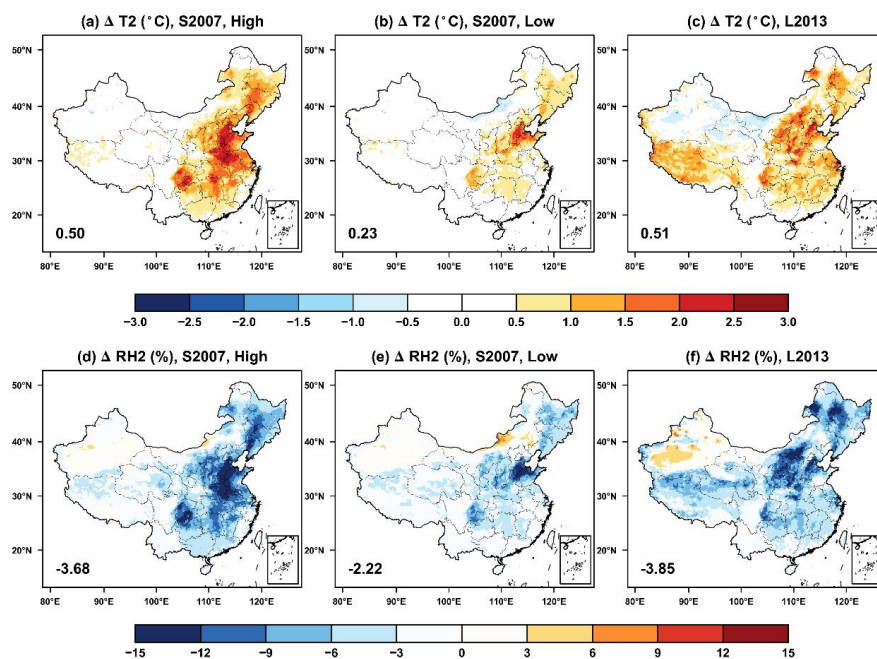
724  
725  
726  
727  
728  
729  
730

**Figure 4** Offline O<sub>3</sub> damage (%) to the (a-c) gross primary productivity (GPP) and (d-f) transpiration rate (TR) predicted by the Sitch scheme with (a, d) high and (b,e) low sensitivities or the (c, f) Lombardozzi scheme. The area-weighted percentage changes are shown in the lower left corner.



731  
732  
733  
734  
735  
736  
737  
738

**Figure 5** The feedback of O<sub>3</sub>-vegetation interaction to surface (a-c) sensible and (d-f) latent heat fluxes in the summer predicted by the S2007 scheme with (a, d) high and (b, e) low sensitivities or the (c, f) L2013 scheme. The relative changes are shown with area-weighted percentage changes indicated at the lower left corner.

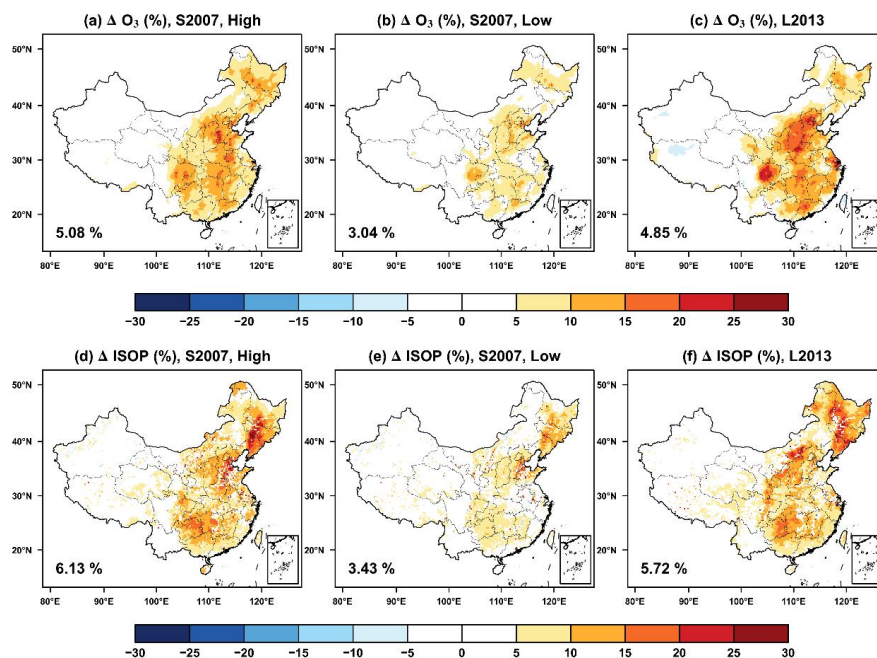


739  
740  
741  
742  
743  
744

**Figure 6** The same as Figure 5 but for changes in (top) air temperature and (bottom) relative humidity at 2 meters.



745



746

747

748

749

750

751

752

753

**Figure 7** The feedback of O<sub>3</sub>-vegetation interaction to surface O<sub>3</sub> concentrations and isoprene emissions in the summer predicted by the S2007 scheme with (a, d) high and (b, e) low sensitivities or the (c, f) L2013 scheme. The area-weighted percentage changes are shown in the lower left corner.